Inorganic–Organic Hybrids

International Edition: DOI: 10.1002/anie.201812554
German Edition: DOI: 10.1002/ange.201812554

# From Lead Iodide to a Radical Form Lead-Iodide Superlattice: High Conductance Gain and Broader Band for Photoconductive Response

*Guan-E Wang, Gang Xu, Ning-Ning Zhang, Ming-Shui Yao, Ming-Sheng Wang,* and Guo-Cong Guo*

*Dedicated to Prof. Jin-Shun Huang on the occasion of his 80th birthday*

***Abstract:*** *Superlattice materials offer new opportunities to modify optical and electrical properties of recently emerging 2D materials. The insertion of tetraethylbenzidine (EtDAB) into interlamination of the established 2D $PbI_2$ semiconductor through a mild solution method yielded the first lead iodide superlattice, $EtDAB{\cdot}4PbI_2$ (EtDAB = tetraethylbenzidine), with radical and non-radical forms. The non-radical form has a non-ionic structure that differs from the common ionic structures for inorganic–organic hybrid lead halides. The radical form shows five orders of magnitude greater conductance and broader photoconductive response range (UV/Vis → UV/Vis-IR), than pure $PbI_2$ and the non-radical form of the superlattice.*

Two-dimensional (2D) layered materials, such as graphene, molybdenum disulfide, and metal–organic frameworks (MOFs),[1] have unique physical and chemical properties and many potential applications in electronics,[2] biomedicine,[3] electrochemical energy storage,[4] chemical sensing/biosensing,[5] and catalysis.[6] Inserting them with neutral alkali metal, alkaline earth, rare earth or organic groups can yield intercalation compounds cohered by van der Waals interactions, the so-called superlattices,[7] which offers new opportunities to modify optical and electrical properties of the host 2D material.[8] For example, superconductivity was discovered not for pure graphite but for a graphite superlattice with intercalated $C_6Ca$ (transition temperature, 11.5 K);[9] optical transmission and electrical conductivity of the 2D $MoS_2$ material were substantially improved when Li was intercalated;[7a] an On/Off current ratio exceeding $10^7$ was observed for a transistor fabricated with a cetyltrimethylammonium bromide-intercalated phosphorene superlattice.[10] To date, the host 2D materials for artificial superlattices are still limited to graphenes, transition-metal oxides/dichalcogenides,[7a,c,11] phosphorenes,[10] and carbides.[9,12] Lead-halide-based organic–inorganic hybrid materials have attracted considerable interest owing to their novel electrical properties and promising applications in perovskite solar cells.[13] However, there is little information on lead-halide-based superlattices.

We herein present the first lead-iodide superlattice, $EtDAB{\cdot}4PbI_2$ (**1**; EtDAB = tetraethylbenzidine), which has radical (**1-G**, green) and non-radical (**1-Y**, yellow) forms. Inorganic–organic hybrid lead halides are usually built from organic cations and lead-halide anion, however, the non-radical form **1-Y** has a non-ionic structure. Biphenylamine and its derivatives are good electron receptors, and absorption bands of their radical products cover a region ranging from UV to near IR.[14] Inserting them between $PbI_2$ layers offers a chance to modify electron structure and corresponding electrical properties. As expected, conductivity ($\sigma$) of the radical form **1-G** is almost 5 orders of magnitude greater than those of the non-radical form **1-Y** and pure $PbI_2$. Furthermore, the cutoff response of photoconductance is located in the visible region (ca. 560 nm) for $PbI_2$[15] but extended to the IR range (for example 1800 nm) after formation of the superlattice.

The superlattice **1** was obtained by an antisolvent diffusion method: a solution of 0.0231 g of $PbI_2$ (0.05 mmol) and 0.0059 g of EtDAB (0.02 mmol) in 3 mL DMF was placed into a $CH_3CN$ atmosphere. After 2 weeks, the radical form **1-G**, was obtained (yield 90% based on $PbI_2$) as crystals with sizes several dozens of micrometers (Figure S1 in the Supporting Information). The usual methods to confirm the superlattice structure are powder X-ray diffraction (PXRD) and cross-sectional transmission electron microscopy (TEM).[10] We used, for the first time, the single-crystal X-ray diffraction analysis to study the superlattice structure. The diffraction data showed that **1** belongs to the monoclinic system with a space group of $C2/m$ ($a = 7.94$ Å, $b = 4.59$ Å, $c = 13.40$ Å, $\beta = 95.75°$, $V = 485.8(2)$ Å$^3$). Selected area electron diffractions (SAED) of one fragment of the radical form **1-G** also match the monoclinic crystal structure, further confirming the crystalline phase (Figure S2). The inorganic part of **1** was easily solved. It has a similar structure to the known neutral layered $PbI_2$[16] (Figure 1 a) with space group of $P\bar{3}m1$. Each Pb atom is coordinated by six I atoms, yielding a slightly distorted octahedral configuration (Figure S3). The [$PbI_6$] octahedra connect to each other in the edge-sharing mode to form a 2D layered structure. The electron density map (Figure S4) showed that there was no residual electron density between two adjacent $PbI_2$ layers, indicating the

[*] Dr. G.-E Wang, Prof. Dr. G. Xu, Dr. N.-N. Zhang, Dr. M.-S. Yao, Prof. Dr. M.-S. Wang, Prof. Dr. G.-C. Guo
State Key Laboratory of Structural Chemistry, Fujian Institute of Research on the Structure of Matter, Chinese Academy of Sciences
Yangqiao west road 155#, Fuzhou, Fujian 350002 (China)
E-mail: mswang@fjirsm.ac.cn
Supporting information and the ORCID identification number(s) for the author(s) of this article can be found under: https://doi.org/10.1002/anie.201812554.

  

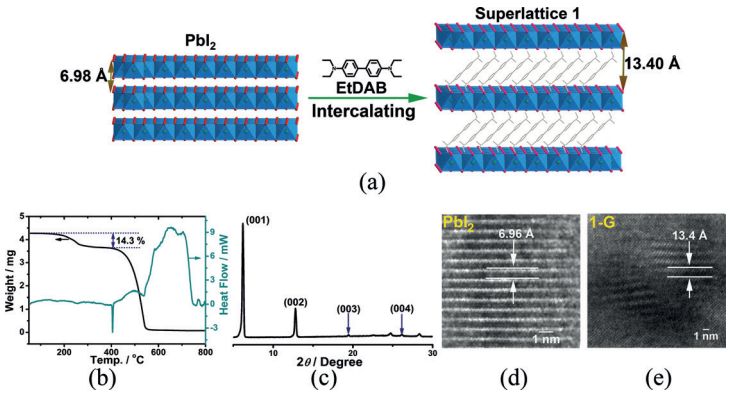


***Figure 1.*** Superlattice **1** in the radical form (**1-G**): a) synthesis, b) thermogravimetric curve, c) powder X-ray diffraction pattern, and e) high-resolution cross-sectional TEM image. High-resolution cross-sectional TEM image for $PbI_2$ (d) is also included for comparison.

interlayer part is highly disordered. ESI-MS (Figure S5) and NMR data (Figure S6) demonstrated that the disordered part is exclusively the EtDAB molecules. As shown in Figure 1 b, the as-synthesized sample of **1** (**1-G**) exhibited a weight loss of about 14.3 % from 200 to 300 °C, corresponding to the formula of EtDAB·4$PbI_2$. Elemental analysis of C, H, N further demonstrated this composition (Table S1 in the ESI). In the pure $PbI_2$, the $PbI_2$ layers stack along the *c* direction through van der Waals interactions, giving the nearest interlayer distance of 6.98 Å (Figure 1 a). In **1**, the distance between two adjacent $PbI_2$ layers is 13.40 Å (Figure 1 a), consistent with the calculated 13.34 Å at $2\theta = 6.62°$ on the basis of PXRD data (Figure 1 c). Cross-sectional high resolution transmission electron microscopy (TEM) also show a clearly resolved expansion of interlayer distance from 6.96 Å in the known layered $PbI_2$ (Figure 1 d) to 13.40 Å in **1** (Figure 1 e).

An electron spin resonance (ESR) study indicated that the radical form **1-G** showed a single-line symmetric signal with a *g* value of 2.002 and a linewidth of 13 Gauss (Figure 2 b), which remained nearly constant in the temperature range of 290–350 K in 2 months (Figure S7). The signal is similar to that of the radical of the EtDAB (tetraethylbenzidine) analogue, tetramethylbenzidine.[14] **1-G** has three broad bands at approximately 390, 750 and 1350 nm in the UV/Vis/NIR diffuse reflectance absorption spectrum (Figure 2 c). The 390 nm band covers the intrinsic absorption bands of pure $PbI_2$ and pure EtDAB (Figure S8), indicating the contribution of both $PbI_2$ and EtDAB. The 750 and 1350 nm bands are close to the electron absorption bands of $EtDAB^{\bullet-}$ radical calculated at the B3LYP/6-31G(d,p) level using an optimized geometry (Figure S9), and thus can be ascribed to the EtDAB radical.

As shown in Figure 2 a, the as-synthesized radical form **1-G** which is green easily changed to the non-radical form **1-Y** which is yellow through thermal annealing at 100 °C for about 1 hour in air/Ar. The generation of a non-radical product was demonstrated by disappearance of ESR radical signal and absorption peaks at 750 and 1350 nm (Figure 2 b,c). IR (Figure S10), NMR (Figure S11) spectroscopy data revealed that molecular structure of the organic component was not destroyed and the change was tiny. PXRD analyses showed that **1-G** and **1-Y** have similar crystal structures (Figure 2 d). That is to say, the non-radical form **1-Y** is exclusively constructed by neutral molecules, including layered $PbI_2$ and EtDAB. Normally, inorganic–organic hybrid lead halides are formed from organic cations and lead-halide anion,[17] which are stacked through Coulomb interactions instead of van der Walls interactions.

An in situ X-ray photoelectron spectroscopy (XPS) study of **1-G** and **1-Y** was performed to reveal the formation mechanism of radicals in **1-G**. The data revealed that Pb 4f core-level spectra of both samples did not show clear peak shift (Figure S12a), which indicates that Pb atoms did not lose or receive electrons. As for C 1s and N 1s core-level spectra

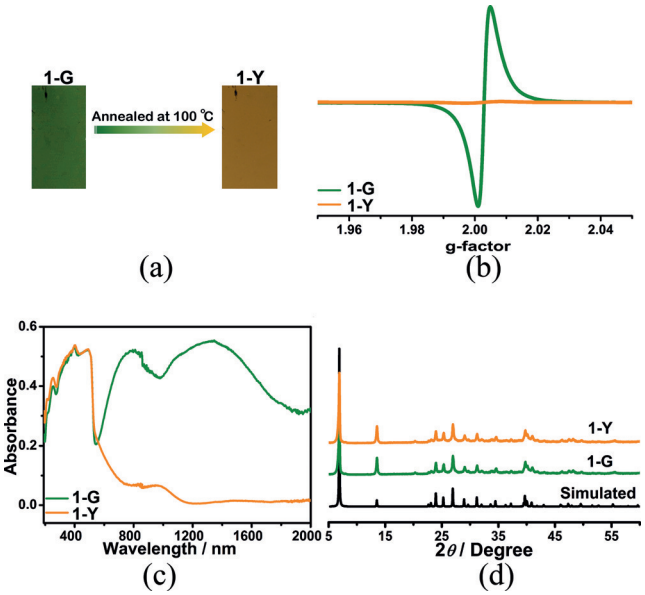


***Figure 2.*** a) The conversion of radical form **1-G** to non-radical form **1-Y**. b) ESR spectra of **1-G** and **1-Y**. c) UV/Vis-NIR spectra of **1-G** and **1-Y**. d) PXRD patterns of **1-G** and **1-Y** with simulated data for comparison.

(Figure S12b and S12c), the peaks of high and low binding energies became stronger and weaker, respectively, when the radical form **1-G** changed to the non-radical form **1-Y**. Therefore, the EtDAB molecules in **1-G** should receive electrons and exist as $EtDAB^{\bullet-}$ radical form. This result is consistent with the above conclusion drew from the UV/Vis-NIR absorption and ESR data (Figure 2 b, c). As for the I 3d core-level spectra (Figure S12d), both I $3d_{5/2}$ and $3d_{3/2}$ peaks shifted to positions with higher binding energies when **1-G** changed to **1-Y**. That is to say, the I atoms in **1-G** should lose electrons.

The difference of electrical conductivity ($\sigma$) between pure layered $PbI_2$ and the superlattice **1** was investigated in vacuum by the two probe method using pressed pellet.[18] As shown in Figure 3 a, the conductivity of pure $PbI_2$ along the layer is $1.07 \times 10^{-9}$ S cm$^{-1}$ at 300 K. The non-radical form **1-Y** shows a similar $\sigma$ value ($8.28 \times 10^{-10}$ S cm$^{-1}$) with that of $PbI_2$

  

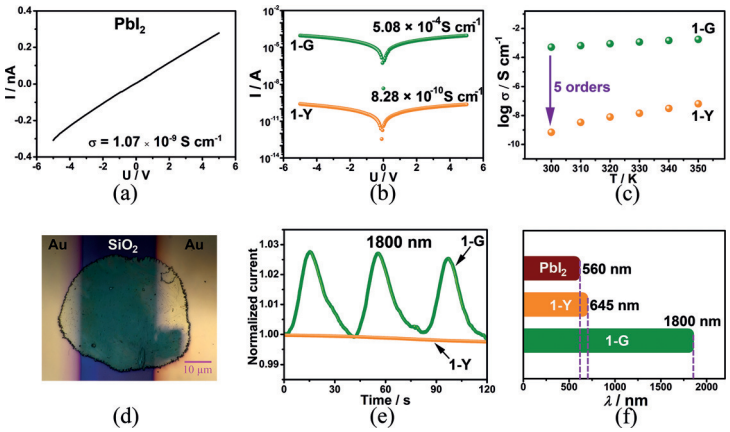


***Figure 3.*** a) *I–V* curve of pure layered $PbI_2$ at 300 K measured using a pressed pellet. b) *I–V* curves of **1-G** and **1-Y** at 300 K. c) Temperature-dependent conductivity plots of **1-G** and **1-Y**. d) Photograph of the single crystal of **1-G** for electrical study. e) Photocurrent responses of **1-G** and **1-Y** irradiated by 1800 nm laser with energy of 0.60 mJ. f) Photoconductive response band for $PbI_2$, **1-Y**, and **1-G**.

(Figure 3b). Layered $PbI_2$ is a typical p-type semiconductor[19] and the main carriers for conducting are holes. As for the radical form **1-G**, electron transfer from layered $PbI_2$ to EtDAB increases the hole concentration in the layered $PbI_2$ and thus $\sigma$ should be larger than that of **1-Y**. The experimental data, recorded using four samples, completely supports this prediction. The four sets of data are similar (Figure 3 and Figure S16), and thus only one set of data is described here. The $\sigma$ value of the radical form **1-G** is $5.08\times10^{-4}\,S\,cm^{-1}$, which is approximately 5 orders of magnitude greater than that of pure $PbI_2$ and the non-radical form **1-Y**. In the temperature range of 300–350 K, the conductivities for both forms of **1** became larger with the increase of temperature, showing semiconductive properties (Figure 3c). As for the radical form **1-G**, electron transfer from layered $PbI_2$ to EtDAB increases the hole concentration in the layered $PbI_2$ and thus $\sigma$ should be larger than that of **1-Y**.

Broad electron absorption band is highly desirable for real application of a light absorber on solar cells.[20] As described above, absorption range of the radical form **1-G** is significantly wider than those of the non-radical form **1-Y** and pure layered $PbI_2$. Such broadband absorption means that there may be a larger photoconductive response range. In order to avoid the problem of light penetration caused by lamination, we used a single-crystal electrode to measure the photoconductivity of **1**. The main challenge of working with a single crystal is its small size (less than 100 μm in this case), and using gold or silver paste will easily lead to short-circuit of the device. The short-circuit problem was addressed by evaporating electrodes on both sides of the crystal and testing both the bulk conductivity and the photoconductivity on the same single crystal for each of the two forms (Figure 3d). The thickness of one typical single-crystal electrode, confirmed by AFM, was approximately 500 nm (Figure S13). Note that the recorded $\sigma$ value for this electrode is comparable to that of the pellet sample (Figure S14). A Xe lamp (ca. 100 $mW\,cm^{-2}$) covered by one bandpass filter ($450\pm40$ nm; $590\pm40$ nm; $\geq645$ nm) and an OPO laser were used for measurement of the photoconductive response range. Both **1-G** and **1-Y** showed photocurrent response to the radiation wavelength of less than 590 nm (Figure S15). When the irradiation wavelength is longer than 645 nm, for example 1800 nm from the OPO laser, only **1-G** still has a photocurrent response though the value of photocurrent is low (Figure 3e and Figure S15). The same case was observed in additional three samples (Figure S17). That is to say, the photocurrent response is limited to the UV/Vis range for the non-radical **1-Y** and pure $PbI_2$ but extends to the infrared region for the radical form **1-G** (Figure 3f). As mentioned above (Figure 2c), the expansion of electron absorption band "for the radical form **1-G** was mainly due to the EtDAB radicals. Therefore, modifying the organic part between two $PbI_2$ layers is a potential approach to improve the photoconductive response range of the superlattice.

In conclusion, we have synthesized the first lead iodide superlattice. It has radical and non-radical forms. The non-radical form has a non-ionic structure that differs from the common ionic structure for inorganic–organic hybrid lead halides. The conductivity of the radical form is about 5 orders of magnitude greater than that of pure $PbI_2$ and the non-radical form. In addition, the photoconductive response range of pure $PbI_2$ and the non-radical form is limited to the UV/Vis range, while that of the radical form extends to the infrared region. This work not only enriches the lead halide family but provides a potential approach to improve conductivity and photoconductivity of 2D materials.

## Acknowledgements

This work was supported by the National Key R&D Program of China (2017YFA0206802), Natural Science Foundation of Fujian Province (2017J05034, 2016J06006), the Strategic Priority Research Program, CAS (XDB20000000), Key Research Program of Frontier Science, CAS (QYZDB-SSW-SLH023, QYZDB-SSW-SLH020), National Natural Science Foundation of China (21822109, 21773245, 21801243), Scientific Research and Equipment Development Project of CAS (YZ201609), Youth Innovation Promotion Association CAS.

## Conflict of interest

The authors declare no conflict of interest.

**Keywords:** inorganic–organic hybrids · lead halides · radicals · semiconductors · superlattices

**How to cite:** *Angew. Chem. Int. Ed.* **2019**, *58*, 2692–2695
*Angew. Chem.* **2019**, *131*, 2718–2721

  

[1] a) X. J. Li, J. H. Yu, K. Luo, Z. H. Wu, W. Yang, *Nanotechnology* **2018**, *29*, 174001; b) X. Fan, P. Xu, Y. C. Li, D. Zhou, Y. Sun, M. A. Nguyen, M. Terrones, T. E. Mallouk, *J. Am. Chem. Soc.* **2016**, *138*, 5143 – 5149; c) C. Tan, X. Cao, X. J. Wu, Q. He, J. Yang, X. Zhang, J. Chen, W. Zhao, S. Han, G. H. Nam, M. Sindoro, H. Zhang, *Chem. Rev.* **2017**, *117*, 6225 – 6331; d) M. Wu, J. Rhee, T. J. Emge, H. Yao, J. H. Cheng, S. Thiagarajan, M. Croft, R. Yang, J. Li, *Chem. Commun.* **2010**, *46*, 1649 – 1651; e) X.-Q. Qiao, Z.-W. Zhang, D.-F. Hou, D.-S. Li, Y. Liu, Y.-Q. Lan, J. Zhang, P. Feng, X. Bu, *ACS Sustainable Chem. Eng.* **2018**, *6*, 12375 – 12384.

[2] a) Z. Wang, X. He, X. X. Zhang, H. N. Alshareef, *Adv. Mater.* **2016**, *28*, 9133 – 9141; b) H. Chen, S. Dong, M. Bai, N. Cheng, H. Wang, M. Li, H. Du, S. Hu, Y. Yang, T. Yang, F. Zhang, L. Gu, S. Meng, S. Hou, X. Guo, *Adv. Mater.* **2015**, *27*, 2113 – 2120; c) B. Liu, A. Abbas, C. Zhou, *Adv. Electron. Mater.* **2017**, *3*, 1700045; d) X. Wang, P. Wang, J. Wang, W. Hu, X. Zhou, N. Guo, H. Huang, S. Sun, H. Shen, T. Lin, M. Tang, L. Liao, A. Jiang, J. Sun, X. Meng, X. Chen, W. Lu, J. Chu, *Adv. Mater.* **2015**, *27*, 6575 – 6581; e) E. Zhang, P. Wang, Z. Li, H. Wang, C. Song, C. Huang, Z. G. Chen, L. Yang, K. Zhang, S. Lu, W. Wang, S. Liu, H. Fang, X. Zhou, H. Yan, J. Zou, X. Wan, P. Zhou, W. Hu, F. Xiu, *ACS Nano* **2016**, *10*, 8067 – 8077; f) J. Chu, F. Wang, L. Yin, L. Lei, C. Yan, F. Wang, Y. Wen, Z. Wang, C. Jiang, L. Feng, J. Xiong, Y. Li, J. He, *Adv. Funct. Mater.* **2017**, *27*, 1701342.

[3] J. I. Paredes, S. Villar-Rodil, *Nanoscale* **2016**, *8*, 15389 – 15413.

[4] a) J. Wu, J. Peng, Z. Yu, Y. Zhou, Y. Guo, Z. Li, Y. Lin, K. Ruan, C. Wu, Y. Xie, *J. Am. Chem. Soc.* **2018**, *140*, 493 – 498; b) M. Acerce, E. K. Akdogan, M. Chhowalla, *Nature* **2017**, *549*, 370 – 373.

[5] Y. Liu, X. Dong, P. Chen, *Chem. Soc. Rev.* **2012**, *41*, 2283 – 2307.

[6] a) W. Shi, L. Cao, H. Zhang, X. Zhou, B. An, Z. Lin, R. Dai, J. Li, C. Wang, W. Lin, *Angew. Chem. Int. Ed.* **2017**, *56*, 9704 – 9709; *Angew. Chem.* **2017**, *129*, 9836 – 9841; b) X. Fan, G. Zhang, F. Zhang, *Chem. Soc. Rev.* **2015**, *44*, 3023 – 3035.

[7] a) F. Xiong, H. Wang, X. Liu, J. Sun, M. Brongersma, E. Pop, Y. Cui, *Nano Lett.* **2015**, *15*, 6777 – 6784; b) K. J. Koski, J. J. Cha, B. W. Reed, C. D. Wessells, D. Kong, Y. Cui, *J. Am. Chem. Soc.* **2012**, *134*, 7584 – 7587; c) J. Guo, S. Jin, G. Wang, S. Wang, K. Zhu, T. Zhou, M. He, X. Chen, *Phys. Rev. B* **2010**, *82*, 180520; d) S. J. Haigh, A. Gholinia, R. Jalil, S. Romani, L. Britnell, D. C. Elias, K. S. Novoselov, L. A. Ponomarenko, A. K. Geim, R. Gorbachev, *Nat. Mater.* **2012**, *11*, 764 – 767; e) J. P. Motter, K. J. Koski, Y. Cui, *Chem. Mater.* **2014**, *26*, 2313 – 2317; f) Q. Dai, U. Lüders, R. Frésard, U. Eckern, U. Schwingenschlögl, *Adv. Mater. Interfaces* **2018**, *5*, 1701169; g) K. S. Novoselov, A. Mishchenko, A. Carvalho, A. H. Castro Neto, *Science* **2016**, *353*, aac9439.

[8] a) E. Morosan, H. W. Zandbergen, B. S. Dennis, J. W. G. Bos, Y. Onose, T. Klimczuk, A. P. Ramirez, N. P. Ong, R. J. Cava, *Nat. Phys.* **2006**, *2*, 544 – 550; b) C. H. Lee, G. H. Lee, A. M. van der Zande, W. Chen, Y. Li, M. Han, X. Cui, G. Arefe, C. Nuckolls, T. F. Heinz, J. Guo, J. Hone, P. Kim, *Nat. Nanotechnol.* **2014**, *9*, 676 – 681.

[9] T. E. Weller, M. Ellerby, S. S. Saxena, R. P. Smith, N. T. Skipper, *Nat. Phys.* **2005**, *1*, 39 – 41.

[10] C. Wang, Q. He, U. Halim, Y. Liu, E. Zhu, Z. Lin, H. Xiao, X. Duan, Z. Feng, R. Cheng, N. O. Weiss, G. Ye, Y. C. Huang, H. Wu, H. C. Cheng, I. Shakir, L. Liao, X. Chen, W. A. Goddard III, Y. Huang, X. Duan, *Nature* **2018**, *555*, 231 – 236.

[11] a) W. J. Yu, Z. Li, H. Zhou, Y. Chen, Y. Wang, Y. Huang, X. Duan, *Nat. Mater.* **2013**, *12*, 246 – 252; b) K. Kaminaga, D. Oka, T. Hasegawa, T. Fukumura, *J. Am. Chem. Soc.* **2018**, *140*, 6754 – 6757; c) G. Zhou, F. Jiang, J. Zang, Z. Quan, X. Xu, *ACS Appl. Mater. Interfaces* **2018**, *10*, 1463 – 1467.

[12] F. Withers, O. Del Pozo-Zamudio, A. Mishchenko, A. P. Rooney, A. Gholinia, K. Watanabe, T. Taniguchi, S. J. Haigh, A. K. Geim, A. I. Tartakovskii, K. S. Novoselov, *Nat. Mater.* **2015**, *14*, 301 – 306.

[13] a) J. Gong, M. Yang, D. Rebollar, J. Rucinski, Z. Liveris, K. Zhu, T. Xu, *Adv. Mater.* **2018**, *30*, 1800973; b) M. Li, C. Zhao, Z.-K. Wang, C.-C. Zhang, H. K. H. Lee, A. Pockett, J. Barbé, W. C. Tsoi, Y.-G. Yang, M. J. Carnie, X.-Y. Gao, W.-X. Yang, J. R. Durrant, L.-S. Liao, S. M. Jain, *Adv. Energy Mater.* **2018**, *8*, 1801509; c) J. Feng, X. Zhu, Z. Yang, X. Zhang, J. Niu, Z. Wang, S. Zuo, S. Priya, S. F. Liu, D. Yang, *Adv. Mater.* **2018**, *30*, 1801418; d) N. J. Jeon, J. H. Noh, Y. C. Kim, W. S. Yang, S. Ryu, S. I. Seok, *Nat. Mater.* **2014**, *13*, 897 – 903; e) G. Hodes, *Science* **2013**, *342*, 317 – 318; f) M. M. Lee, J. Teuscher, T. Miyasaka, T. N. Murakami, H. J. Snaith, *Science* **2012**, *338*, 643 – 647; g) A. Leblanc, N. Mercier, M. Allain, J. Dittmer, V. Fernandez, T. Pauporte, *Angew. Chem. Int. Ed.* **2017**, *56*, 16067 – 16072; *Angew. Chem.* **2017**, *129*, 16283 – 16288.

[14] K. S. M. Kirchgessner, K. R. Gopidas, *J. Org. Chem.* **2006**, *71*, 9849.

[15] M. Tan, C. Hu, Y. Lan, J. Khan, H. Deng, X. Yang, P. Wang, X. Yu, J. Lai, H. Song, *Small* **2017**, *13*, 1702024.

[16] V. Gulia, A. Vedeshwar, N. Mehra, *Acta Mater.* **2006**, *54*, 3899 – 3905.

[17] B. Saparov, D. B. Mitzi, *Chem. Rev.* **2016**, *116*, 4558 – 4596.

[18] L. Sun, S. S. Park, D. Sheberla, M. Dinca, *J. Am. Chem. Soc.* **2016**, *138*, 14772 – 14782.

[19] a) W. Liu, Y.-J. Liu, L. Chen, T. Ye, H.-Z. Chen, H.-Y. Li, *Chin. Chem. Lett.* **2015**, *26*, 504 – 508; b) M. Shkir, S. AlFaify, *Sci. Rep.* **2017**, *7*, 16091.

[20] a) J. Seo, J. H. Noh, S. I. Seok, *Acc. Chem. Res.* **2016**, *49*, 562 – 572; b) Y. Zhou, Z.-J. Yong, K.-C. Zhang, B.-M. Liu, Z.-W. Wang, J.-S. Hou, Y.-Z. Fang, Y. Zhou, H.-T. Sun, B. Song, *J. Phys. Chem. Lett.* **2016**, *7*, 2735 – 2741; c) Y. Zhou, J. Chen, O. M. Bakr, H.-T. Sun, *Chem. Mater.* **2018**, *30*, 6589 – 6613.


Manuscript received: November 1, 2018
Accepted manuscript online: January 7, 2019
Version of record online: January 25, 2019

  